Hindawi Publishing Corporation
Journal of Nanomaterials
Volume 2014, Article ID 725817, 10 pages
http://dx.doi.org/10.1155/2014/725817

Research Article

Ultrasonic-Assisted Synthesis, Characterization, and Optical Properties of Sb Doped ZnO and Their Photocatalytic Activities

Anukorn Phuruangrat,[1] Waipawan Kongpet,[1] Oranuch Yayapao,[2] Budsabong Kuntalue,[3] Somchai Thongtem,[2,4] and Titipun Thongtem[4,5]

[1] *Department of Materials Science and Technology, Faculty of Science, Prince of Songkla University, Hat Yai, Songkhla 90112, Thailand*
[2] *Department of Physics and Materials Science, Faculty of Science, Chiang Mai University, Chiang Mai 50200, Thailand*
[3] *Electron Microscopy Research and Service Center, Faculty of Science, Chiang Mai University, Chiang Mai 50200, Thailand*
[4] *Materials Science Research Center, Faculty of Science, Chiang Mai University, Chiang Mai 50200, Thailand*
[5] *Department of Chemistry, Faculty of Science, Chiang Mai University, Chiang Mai 50200, Thailand*

Correspondence should be addressed to Anukorn Phuruangrat; phuruangrat@hotmail.com and Somchai Thongtem; schthongtem@yahoo.com

Received 3 September 2013; Revised 21 November 2013; Accepted 4 December 2013; Published 5 February 2014

Academic Editor: Zhenhui Kang

Sb doped ZnO nanostructures were synthesized by an ultrasonic-assisted method. Effect of Sb dopant on the structure, morphology, and composition of as-synthesized Sb doped ZnO nanostructures was investigated by X-ray diffraction (XRD), scanning electron microscopy (SEM), energy dispersive X-ray (EDX) spectroscopy, and transmission electron microscopy (TEM). All samples were identified to wurtzite hexagonal ZnO structure. UV-visible spectra of the as-synthesized 3% Sb doped ZnO sample exhibit broad absorption bands at around 343 nm which is blue shift of 373 nm of pure ZnO. The photocatalytic activity was tested by decolorization of methylene blue (MB) solution under UV light. After 300 min irradiation, the degradation efficiencies were 56, 90, and 95% for ZnO, 1% Sb doped ZnO, and 3% Sb doped ZnO, respectively. The 3% Sb doped ZnO shows the highest photocatalytic activity than any other samples.

1. Introduction

Zinc oxide (ZnO) is a n-type II–VI semiconductor with a wide direct band gap of 3.37 eV and large exciton binding energy of 60 meV [1–5], which is more than other semiconductor materials: ZnSe (22 meV) and GaN (25 meV) [6]. It has interesting applications on nanolasers, piezoelectric nanogenerators, solar cells, gas sensors, and photocatalyst, due to its unique optical and electrical properties [1, 2, 4, 7]. However, its electrical and optical properties are not able to completely meet the requirements of constructing high performance semiconducting devices, including the increasing needs for applications nowadays [1, 2, 5]. To enhance these properties, ZnO was frequently doped with some dopants [1, 2, 5] such as Sb [6, 8], Sn [9], In [10, 11], Mn [12], and Ce [13]. Sn doped ZnO shows the highest gas response to ethanol vapor and highest photocatalytic activity toward methyl orange (MO) solution [9]. The 2% Ce doped ZnO shows an effective oxidation of cyanide to cyanate [13]. Sb doped ZnO nanoparticles have higher resistance and reflectivity than the undoped ones [8].

In this research, a facile and environment-friendly low-temperature route was used to synthesize Sb doped ZnO by ultrasonic-assisted solution method. Phase, morphologies, optical properties, and photocatalytic properties of Sb doped ZnO were also studied and discussed in this report.

2. Experimental Procedures

Sb doped ZnO nanostructures were synthesized by the ultrasonic-assisted solution method using zinc nitrate hexahydrate ($Zn(NO_3)_2{\cdot}6H_2O$), antimony chloride ($SbCl_3$), and ammonium hydroxide (NH_4OH) as starting materials. All

the chemicals for this synthesis were purchased from Aldrich Chemical Corporation and used without further purification.

For the typical experimental procedure, 0.01 mol of $Zn(NO_3)_2{\cdot}6H_2O$ and 1–5% by mole of $SbCl_3$ were dissolved in 100 mL of deionized water. Aqueous solution of 28% ammonium hydroxide was dropped in precursor solutions until reaching the pH of 8.5 with continuous stirring to precipitate Zn^{2+} and Sb^{3+} ions into metal hydroxide compound. Subsequently, the resultant solutions were transferred into sonication bath (35 kHz) and sonicated at 80°C for 3 h. In the end, the precipitates were filtered and washed with methanol several times to remove ionic impurities and finally dried at room temperature.

Crystalline phases of the as-synthesized nanostructured materials were analyzed by an X-ray diffractometer (XRD, Philips X'Pert MPD) with Cu-K_α radiation in the 2θ = 15°–75° range. The morphology investigation was carried out by field emission scanning electron microscopy (FE-SEM, JEOL JSM-6335F) and transmission electron microscopy (TEM, JEOL JEM-2010) operating at 35 kV and 200 kV, respectively. The optical properties were studied by a Perkin Elmer, Lambda 25 UV-visible spectrometer.

Photocatalytic activity was tested by decolorization of methylene blue (MB) in aqueous solution under UV light. The 150 mg pure ZnO and Sb doped ZnO as photocatalysts were suspended in 150 mL 10^{-5} M MB solutions and were magnetically stirred for 30 min in the dark environment to establish an adsorption/desorption equilibrium of MB on surfaces of the photocatalysts. After UV irradiating, the concentrations of MB were determined by a UV-visible spectrophotometer (Lambda 25, Perkin Elmer) using a wavelength of 664 nm. The decolorization efficiency (%) was calculated as follows:

$$\text{decolorization efficiency (\%)} = \frac{C_o - C}{C_o} \times 100 \quad (1)$$

where C_o and C were the initial concentration of MB and the concentration of MB after UV irradiation, respectively.

3. Results and Discussion

The purity and crystalline properties of the as-synthesized ZnO and Sb doped ZnO samples were determined by X-ray diffraction (XRD) as shown in Figure 1. The XRD pattern of ZnO without Sb dopant showed diffraction peaks at 2θ = 31.8°, 34.5°, 36.4°, 47.5°, 57.1°, 63.2°, 66.7°, 67.8°, and 69.0°, identified to the (100), (002), (101), (102), (110), (103), (200), (112), and (201) planes, respectively, of bulk wurtzite hexagonal ZnO structure (JCPDS no. 36-1451) [14]. No observed characteristic peaks corresponding to impurities such as $Zn(OH)_2$ were detected in the pattern, confirming the purity of ZnO sample. XRD patterns of 1–3% Sb doped ZnO show the same diffraction pattern as pure wurtzite hexagonal ZnO structure with JCPDS no. 36-1451. no diffraction peaks of impurity phases such as $Zn(OH)_2$, Sb_2O_3, and Sb were detected in these samples, suggesting that Sb^{3+} ions could uniformly substitute into the Zn^{2+} sites or interstitial sites of ZnO lattice by forming $2Sb_{Zn}$ and V_{Zn} [3]. Moreover,

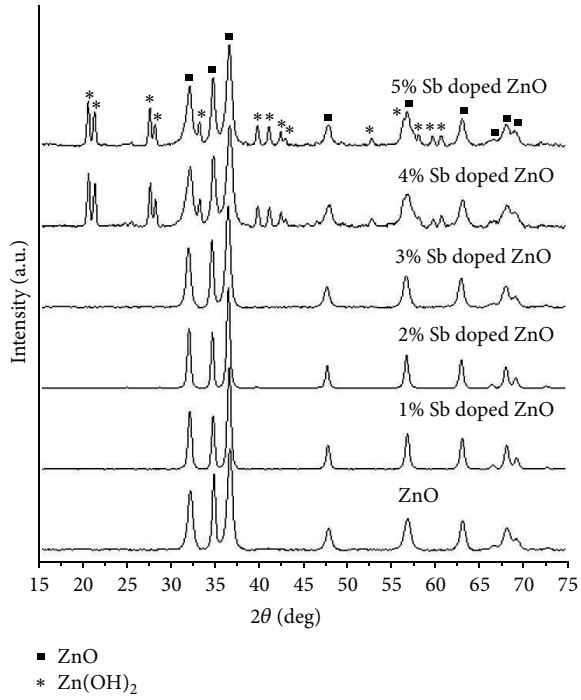

Figure 1: XRD patterns of the products synthesized by ultrasonic-assisted solution method.

the major diffraction peaks shifted slightly towards smaller diffraction angle compared to the pure ZnO phase due to the ionic radius of Sb^{3+} of 0.76 Å [15, 16] >ionic radius of Zn^{2+} of 0.74 Å [16, 17]. Upon increasing the Sb concentration doped in ZnO structure of more than 3%, mixed phases of $Zn(OH)_2$ and ZnO (JCPDS no. 38-0385 [14] for $Zn(OH)_2$ and no. 36-1451 [14] for ZnO) were detected. The XRD results show that the limited Sb concentration doped in ZnO is 3 wt% in this research.

Figures 2 and 3 show the FE-SEM images of the as-synthesized 0–3% Sb doped ZnO products with low and high magnifications. A morphology of pure ZnO as shown in Figure 2(a) was well-defined flower-like three-dimensional ZnO nanostructures in a large-scale area with diameters in the range of 0.5–1 μm. It should be noted that the flower-like three-dimensional ZnO nanostructures were composed of assemblies of nanorods as petals. At high magnification image of the nanorod-built flower-like ZnO nanostructures in Figure 3(a), they revealed that each petal was about 300 nm long and 100 nm in diameter. For the SEM images of Sb doped ZnO, the morphologies of rice kernel-like ZnO nanostructures formed instead of flower-like structures. Figures 2(b), 2(c), and 2(d) and Figures 3(b), 3(c), and 3(d) show SEM images of 1–3% Sb doped ZnO prepared by ultrasonic-assisted solution method at low and high magnifications. They show the rice kernel-like ZnO nanorods in the range of 300–400 nm long. However, no flower-like structures were detected in the Sb doped ZnO samples. At high magnification, the products were composed of assembled nanorods to build rice kernel-like ZnO nanorods. These different morphologies of ZnO and 1–3% Sb doped ZnO can

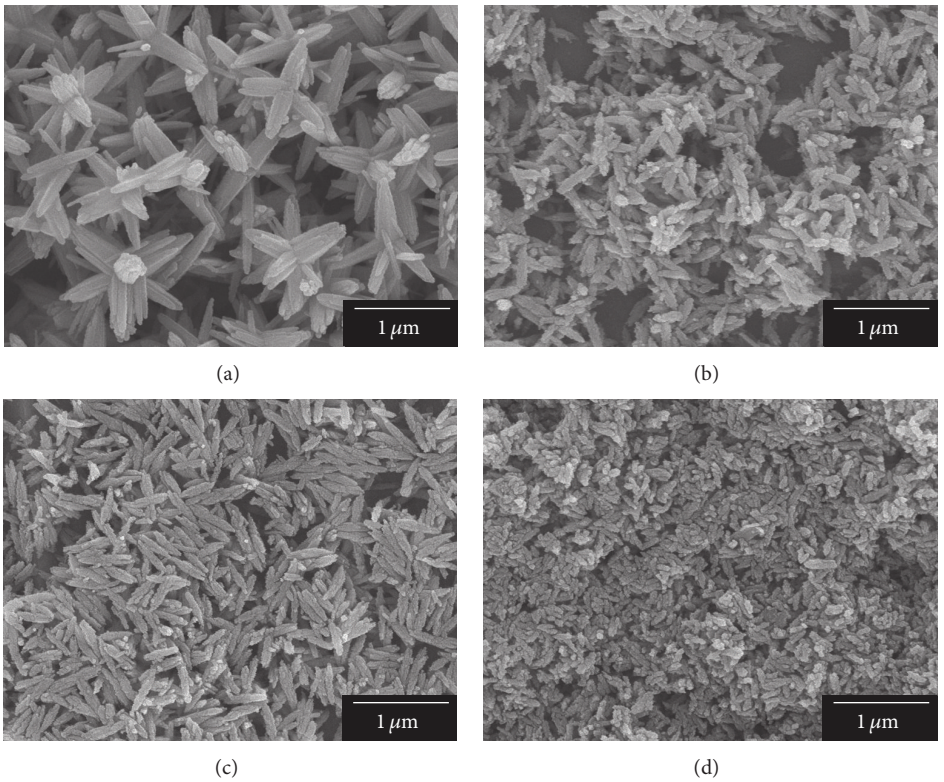

(a) (b)

(c) (d)

Figure 2: SEM images of (a) pure ZnO, (b) 1% Sb doped ZnO, (c) 2% Sb doped ZnO, and (d) 3% Sb doped ZnO samples at low magnification.

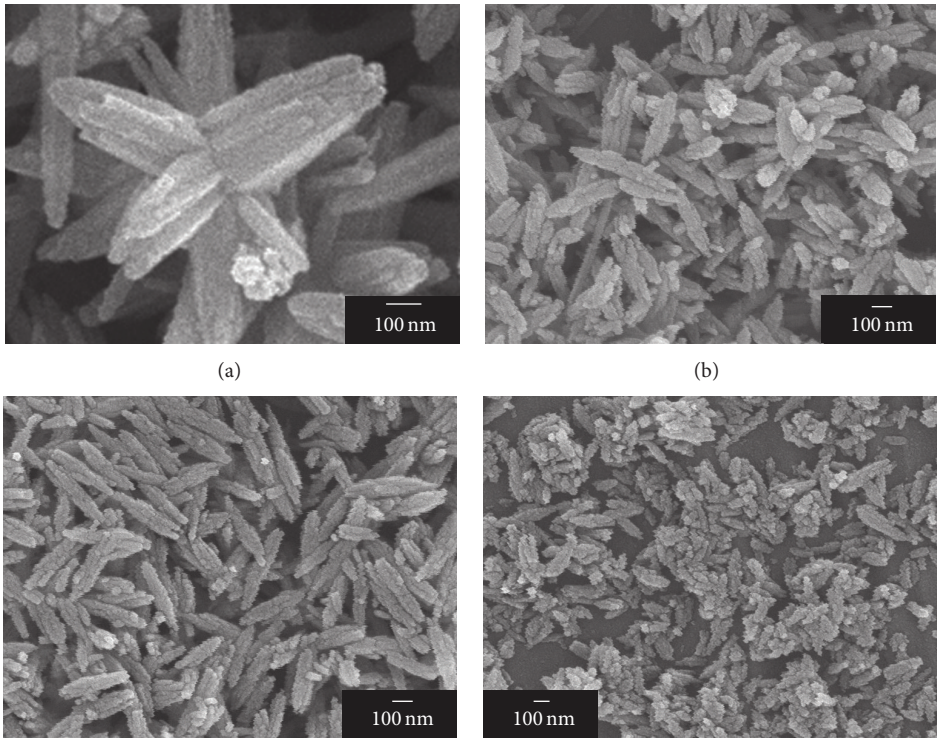

(a) (b)

(c) (d)

Figure 3: SEM images of (a) pure ZnO, (b) 1% Sb doped ZnO, (c) 2% Sb doped ZnO, and (d) 3% Sb doped ZnO samples at high magnification.

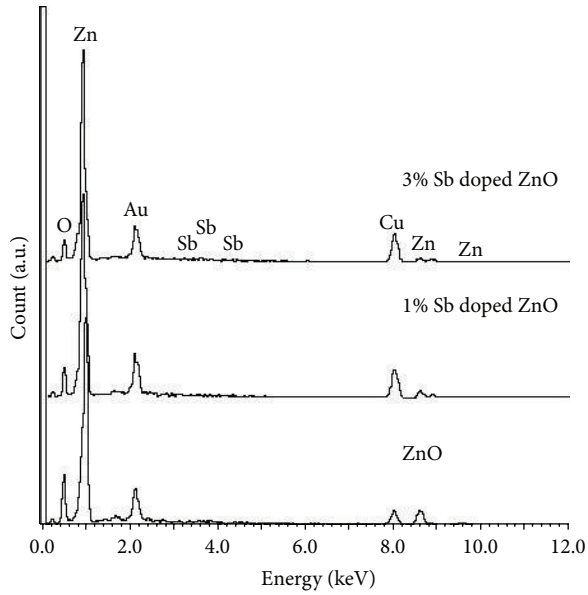

Figure 4: EDX spectra of the products synthesized by ultrasonic-assisted solution method.

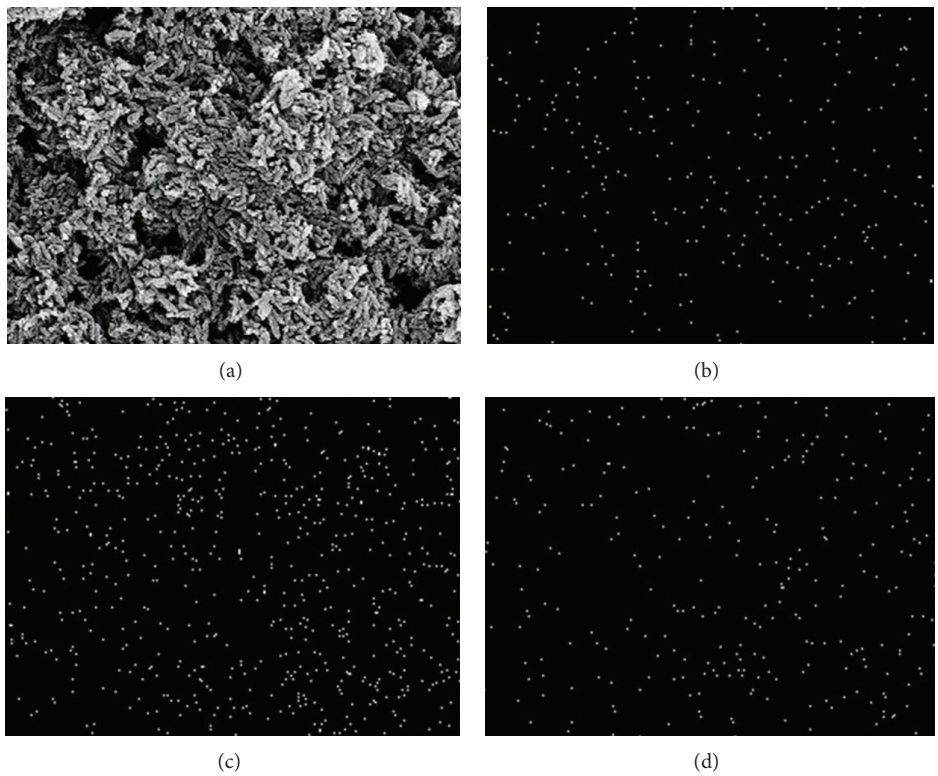

Figure 5: EDX mapping of 3% Sb doped ZnO sample.

be explained in terms of a thermodynamic barrier arising from the Sb^{3+} dopant that slowed down the nucleation and inhibited the further growth of Sb doped ZnO crystals [18].

Chemical composition of the as-synthesized products was observed using EDX analysis. Figures 4 and 5 show the typical EDX spectra of 0–3% Sb doped ZnO and EDX mapping of 3% Sb doped ZnO. EDX spectra show that the products consisted of zinc and oxygen for pure ZnO and zinc, oxygen, and antimony atoms for 1–3% Sb doped ZnO. Intense peaks of Cu and Au were also detected in the spectra due to the Cu stubs and sputtered Au. There was no detection of other impurities in the products, indicating that they had very high purity. Figure 5 shows selected area elemental mapping of 3% Sb doped ZnO. The mapping was

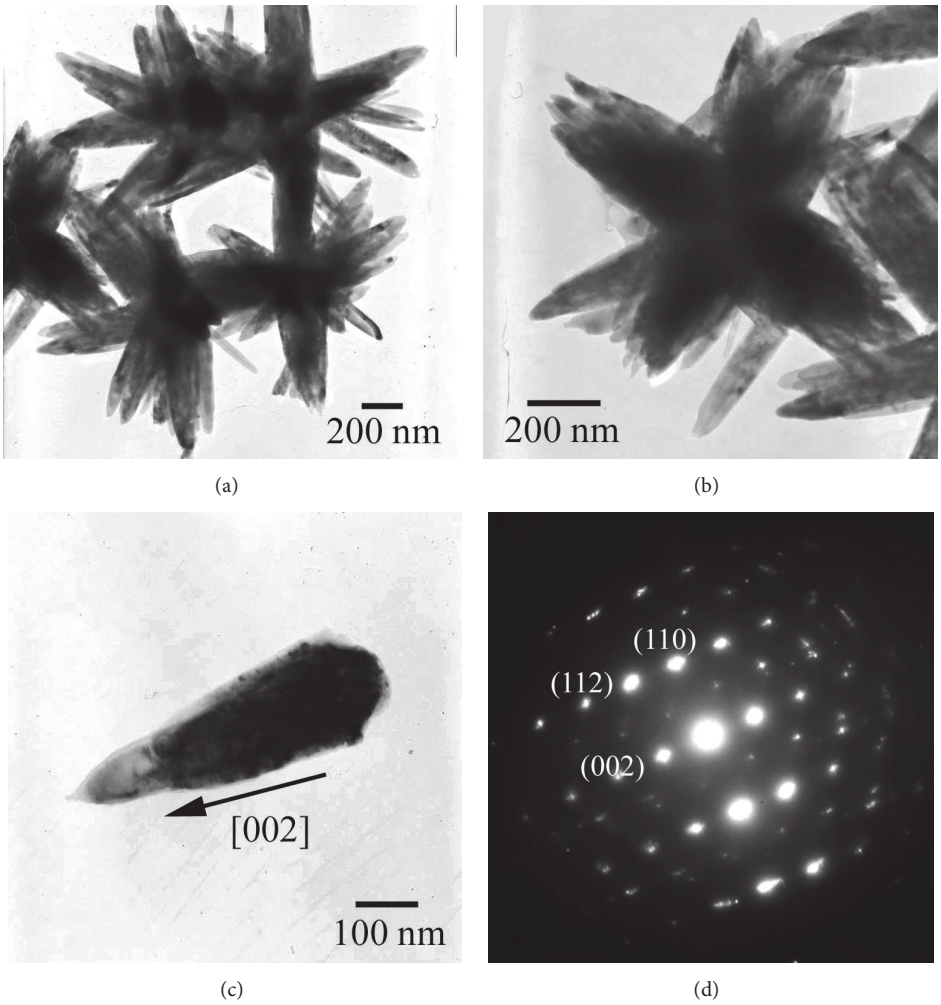

Figure 6: TEM images and SAED pattern of flower-like ZnO structure.

mainly composed of Zn, O, and Sb elements. The Sb element was uniformly diffusive in ZnO lattice.

Figure 6(a) shows a bright-field TEM image of the as-synthesized ZnO sample. It indicates the detailed morphology of the ZnO product with flower-like shape. As shown in Figure 6(b), it can be clearly seen that the detailed shape of some petals of flower-like ZnO product was composed of many clusters ZnO nanorods. These nanorods were in contact with each other as bundles, growing outwardly by forming flower-like structures. The shape of the product appears as flowers with several symmetric petals. It indicated that every bundle was composed of closely packed nanorods with average diameters of around 150 nm. By performing on the individual petal (Figure 6(c)), the selected area electron diffraction (SAED) pattern, as shown in Figure 6(d), indicates that the single petal is single crystal of hexagonal ZnO phase. The individual petal was also confirmed that the nanorods grow along the [0001] direction.

Regarding the formation of flower-like ZnO, it can be explained by manipulating the growth kinetics. In the present case, the contributing growth-driving force for ZnO crystals is the concentration of ZnO_2^{2-} monomers. In the reaction solution containing $Zn(NO_3)_2$ and NH_4OH, the high reactant concentrations led to the burst of initial homogeneous nucleation, and the supersaturated ZnO nuclei aggregated together in groups. As the reaction proceeded, concentration of the ZnO_2^{2-} monomers became lower. Some active sites on the surface of the initially formed ZnO aggregates grew along the oriented direction as the chemical environment constantly provided reactants. Due to the intrinsic anisotropy in its growth rate (v) with $v[0001] \gg v[01\text{-}10] > v[000\text{-}1]$, the preferential growth of the product is along the [0001] direction [7, 19]. The structure of ZnO single crystal can be described as a number of alternating planes of coordinated O^{2-} and Zn^{2+} ions. The oppositely charged ions are made of the positively charged Zn-(0001) and negatively charged O-(0001) polar surfaces. Following the decrease of the concentration of ZnO_2^{2-} monomers due to the initial fast nucleation of ZnO, the absorption of OH^- on the positively charged Zn-(0001) plane dominated the ZnO_2^{2-} growth units. Therefore, the superfluous OH^- ions stabilized the surface charge and the structure of Zn-(0001) face to some degree, allowing

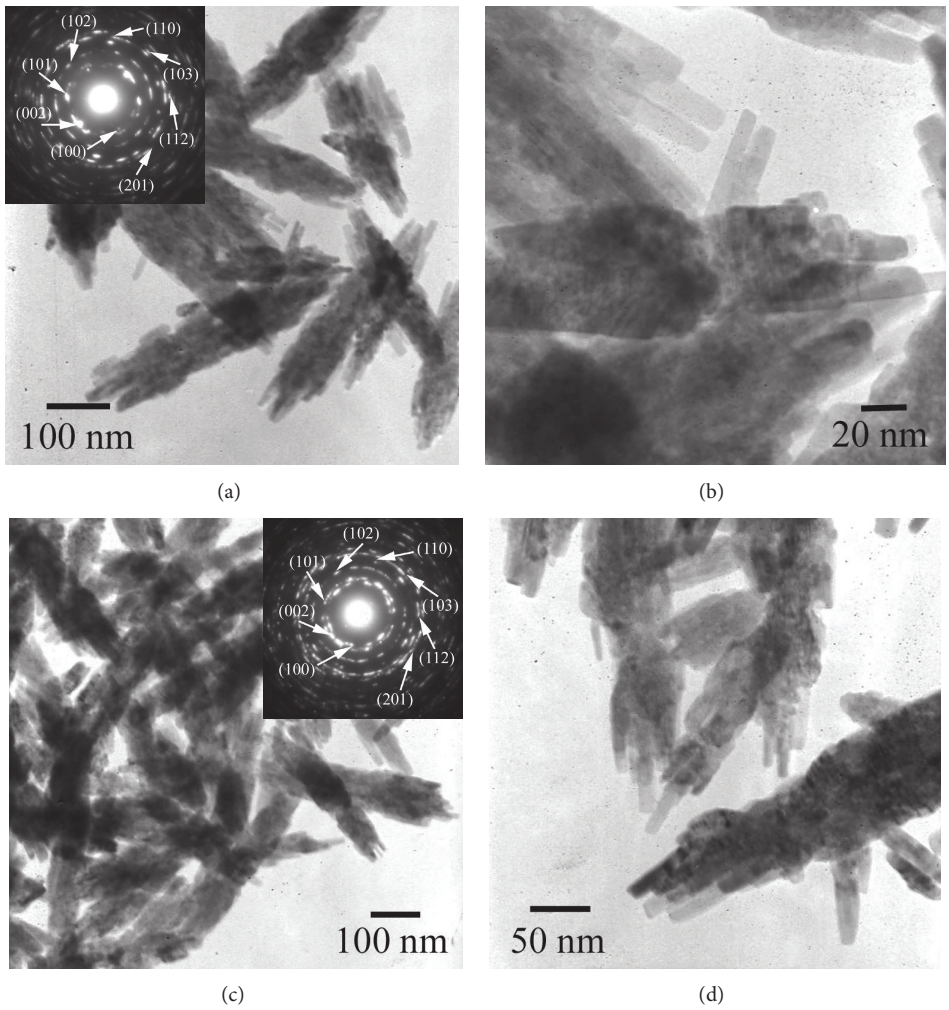

Figure 7: TEM images and SAED patterns of (a) and (b) 1% Sb doped ZnO, and (c) and (d) 3% Sb doped ZnO samples.

the fast growth along the [0001] direction, leading to the formation of flower-like ZnO nanostructure [7, 20–22].

Figure 7 shows the typical TEM images of 1% and 3% Sb doped ZnO nanostructures. It is apparent that 1% Sb doped ZnO exhibits well-defined rice kernel-like colonies with an average size of 300–400 nm. The nanorods serving as building blocks were tightly packed as colonies of rice kernel-like shaped particles. It can be concluded that the rice kernel-like ZnO colonies formed from the attachment of ZnO nanorods. The magnified TEM image in Figure 7(b) shows the detailed colonies of rice kernel-like ZnO. The colonies of rice kernels were composed of densely arrayed nanorods with diameter of about 10 nm. While the colonies of the 3% Sb doped ZnO nanocrystallites as shown in Figure 7(c) present the rice kernel-like colonies of many closely packed nanorods of about 90 nm in diameter and 1.2 μm in length similar to 1% Sb doped ZnO sample. It also shows that the ends of the nanorods have relatively smaller diameters compared to those of the middle parts. The enlarged TEM image of 3% Sb doped ZnO sample as shown in Figure 7(d) shows the colonies of rice kernel-like ZnO particles with very rough surface. It is noteworthy that the rice kernel-like structure was sufficiently stable, which cannot be destroyed even after ultrasonication for a long time. The insets of Figures 7(a) and 7(c) show the SAED pattern taken from their corresponding rice kernel-like Sb-doped ZnO samples. The diffraction patterns were composed of a number of bright spots arranged in concentric rings, with the calculated lattice planes obtained from the diameters of the diffraction rings. For the present research, the products were polycrystalline in nature. They were the (100), (002), (101), (102), (110), (103), (112), and (201) planes which were in accordance with those of the JCPDS database for hexagonal ZnO phase.

The optical properties of as-synthesized 0–3% Sb doped ZnO samples were studied by UV-visible absorption as shown in Figure 8. The spectrum of pure phase ZnO sample exhibits a broad absorption band at around 373 nm, blue shift relative to 380 nm of bulk ZnO [23]. However, the spectra of 1%, 2%, and 3% Sb doped ZnO samples exhibit sharp bands at 356 nm, 350 nm, and 343 nm, respectively. It should be noted that the absorption peaks became sharper. They were blue-shift from 373 nm of pure ZnO sample to 343 nm of

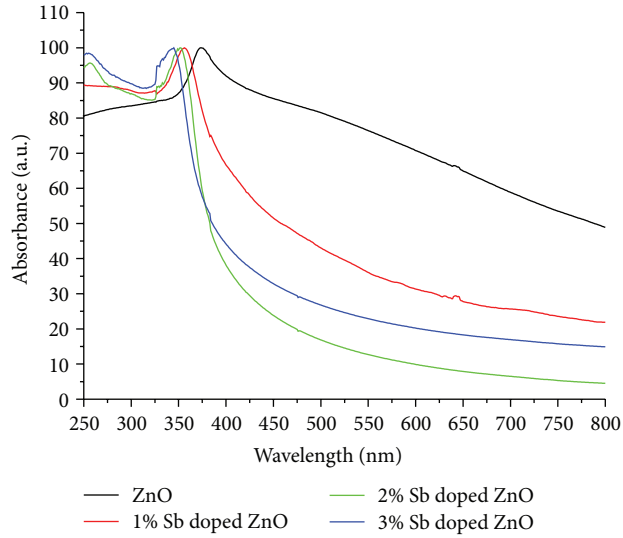

Figure 8: UV-visible spectra of as-synthesized 0–3% Sb doped ZnO samples.

3% Sb doped ZnO sample. The band gaps were calculated by the equation of $E_g = 1240/\lambda$ [24, 25]. They are 3.32 eV, 3.48 eV, 3.54 eV, and 3.61 eV for ZnO, 1% Sb doped ZnO, 2% Sb doped ZnO, and 3% Sb doped ZnO, respectively. These can be explained by the decreasing in size of the particles and consequently the increasing band gap between the valence and conduction bands. A blue shift of the absorption peak in the UV-visible spectra of these samples was successfully and clearly observed.

Upon the illumination of UV light, ZnO can transform the photonic energy into chemical energy, in a similar way for the synthesis or the decomposition of organic materials. Its remarkable oxidation reduction capability, high chemical stability, and harmless characteristics are most commonly applied in pollutant removal and disinfectants. When the ZnO samples are illuminated by ultraviolet of wavelength less than 400 nm, electrons of the valence band were excited by the photonic energy of the ultraviolet to the conduction band. At the same time, the valence band created electronic holes carrying positive electricity. These holes reacted with the absorbed O_2 or H_2O to create $OH^\bullet$ free radicals, which further generated the reaction such as disinfection or deodorization [26]. Figure 9(a) shows the UV-visible absorption spectral change of MB during the photocatalytic degradation in the presence of ZnO under UV light over the wavelength range of 400–800 nm. The intensity of main absorption peaks of the MB solutions at approximately 664 nm decreases continuously with the length of UV irradiation time. It indicates that MB molecules could be degraded in the presence of ZnO. The photocatalytic mechanism of ZnO is as follows:

$$\begin{aligned} \mathrm{ZnO} + \mathrm{hv} &\longrightarrow \mathrm{ZnO}\left(\mathrm{e_{CB}}^- + \mathrm{h_{VB}}^+\right) \\ \mathrm{H_2O} + \mathrm{h_{VB}}^+ &\longrightarrow \mathrm{H}^+ + \mathrm{OH}^\bullet \\ \mathrm{dye} + \mathrm{OH}^\bullet &\longrightarrow \text{oxidation products} \end{aligned} \quad (2)$$

where h_{VB}^+ and e_{CB}^- are the electron vacancies in the valence band and the photogenerated electrons in the conduction band, respectively. The conduction-band electrons and valence-band holes are generated on the surfaces of ZnO nanostructures when they are illuminated by UV light with energy greater than the band gap. Holes react with water molecules adhering to the surfaces of ZnO nanostructures to form highly reactive hydroxyl radicals ($OH^\bullet$) which have a powerful oxidation ability to degrade organic dye [7]. Figures 9(b) and 9(c) show the UV-visible absorption spectra of the aqueous solutions of MB with 1% Sb doped ZnO and 3% Sb doped ZnO samples as photocatalysts and illuminated to UV light for different time intervals. The characteristic absorption of MB at 664 nm decreases rapidly with the prolonging time and almost disappears after about 300 min. Further exposure leads to no absorption peak in the whole spectrum, indicating that almost none of the MB remain. These photocatalysis results clearly demonstrate that Sb doped ZnO exhibited higher photocatalytic activity as compared with ZnO sample.

Figure 10 shows MB degradation efficiency of the as-synthesized ZnO and Sb doped ZnO samples. The Sb doped ZnO samples exhibit much higher photocatalytic activities than that of the pure ZnO one. It took only 102 min for 3% Sb doped ZnO and 134 min for 1% Sb doped ZnO to decolorize 50% of MB while pure ZnO took more than 275 min to decolorize the same amount of MB. This faster degradation rate of MB under UV irradiation using Sb doped ZnO is attributed to the increase in defect sites caused by Sb^{3+} doping, leading to an enhanced optical absorption in the UV region. After 300 min of irradiation, the values of degradation efficiency are 56, 90, and 95% for pure ZnO, 1% Sb doped ZnO, and 3% Sb doped ZnO, respectively. This clearly demonstrates that ZnO doped with Sb^{3+} degrades MB more efficiently than undoped ZnO. In this research, the 3% Sb doped ZnO shows the highest photocatalytic activity. Under illumination with UV light, Sb doped ZnO generates electron-hole pairs at the tail states of conduction and valence bands. The generated

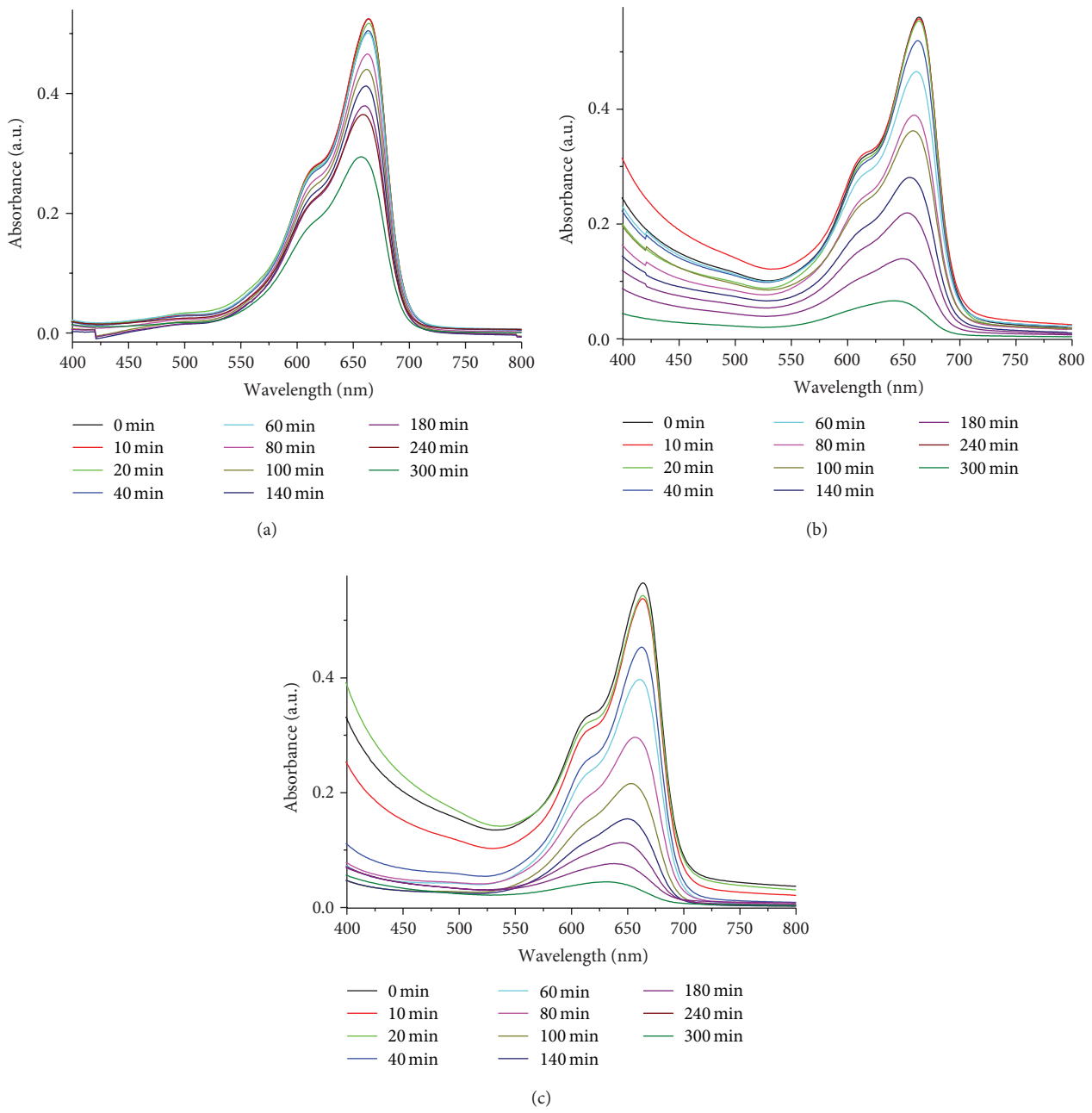

Figure 9: UV-visible absorption of MB solutions containing (a) ZnO, (b) 1% Sb doped ZnO and (c) 3% Sb doped ZnO.

electrons diffused to the adsorbed MB molecules on the surface of Sb doped ZnO. The excited electrons from the photocatalyst conduction band migrated into the molecular structure of MB and by forming the conjugated system which then led to the complete decomposition of MB. Holes at the valence band generated $OH^{\bullet}$ via reaction with water or OH^{-} might be used for oxidation of other organic compounds.

The photocatalytic properties of as-synthesized photocatalysts were evaluated by measuring the absorption intensity of MB at 664 nm after UV irradiation at different lengths of time. Both of these photodegradation reactions were determined by pseudo-first-order reactions [27–30]. The reaction rate constants of MB degradation calculated for ZnO, 1% Sb doped ZnO, and 3% Sb doped ZnO are 1.47×10^{-3}, 6.30×10^{-3}, and 8.65×10^{-3} min^{-1}, respectively. This clearly demonstrates that ZnO doped with antimony can be used as a potential photocatalyst illuminated with UV light.

4. Conclusions

Ultrasonic-assisted synthesis of Sb doped ZnO at room temperature has been introduced. XRD results showed the formation of wurtzite ZnO and the upper bound of 3 wt% doped Sb. No other phases were detected. The amount of

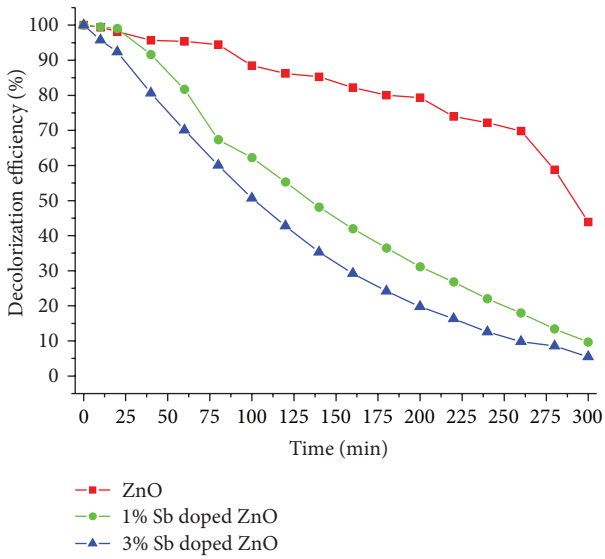

FIGURE 10: Decolorization efficiencies of ZnO with and without Sb doping.

antimony added shows a profound effect on morphology which changed from flower-like structure of nanorods for ZnO to rice kernel-like structure for Sb doped ZnO. As-synthesized doped and undoped ZnO crystals were tested and compared for their photocatalytic activities by decolorization of MB under UV light. It was clear that 3% Sb doped ZnO showed the highest photocatalytic activity toward the MB solution.

Conflict of Interests

The authors declare that there is no conflict of interests regarding the publication of this paper.

Acknowledgment

The authors wish to thank the Thailand Research Fund (TRF) for providing financial support through the TRF research Contract MRG5580112.

References

[1] W.-W. Zhong, F.-M. Liu, L.-G. Cai, X.-Q. Liu, and Y. Li, "Effect of growth time on the structure, Raman shift and photoluminescence of Al and Sb codoped ZnO nanorod ordered array thin films," *Applied Surface Science*, vol. 257, no. 22, pp. 9318–9322, 2011.

[2] D. W. Zeng, C. S. Xie, B. L. Zhu, W. L. Song, and A. H. Wang, "Synthesis and characteristics of Sb-doped ZnO nanoparticles," *Materials Science and Engineering B*, vol. 104, no. 1-2, pp. 68–72, 2003.

[3] X. Fang, J. Li, D. Zhao et al., "Structural and photoluminescence properties of aligned Sb-doped ZnO nanocolumns synthesized by the hydrothermal method," *Thin Solid Films*, vol. 518, no. 20, pp. 5687–5689, 2010.

[4] C. H. Zang, J. F. Su, B. Wang, D. M. Zhang, and Y. S. Zhang, "Photoluminescence of ZnO:Sb nanobelts fabricated by thermal evaporation method," *Journal of Luminescence*, vol. 131, no. 8, pp. 1817–1820, 2011.

[5] W.-W. Zhong, F.-M. Liu, and W.-P. Chen, "Effect of ammonia/zinc nitrate molar ratio on structural and optical properties of Al and Sb codoped ZnO nanorod ordered array thin films," *Journal of Alloys and Compounds*, vol. 531, pp. 59–63, 2012.

[6] S. H. Kim, A. Umar, Y. K. Park, J.-H. Kim, E. W. Lee, and Y. B. Hahn, "Non-catalytic growth of high-aspect-ratio Sb-doped ZnO nanowires by simple thermal evaporation process: structural and optical properties," *Journal of Alloys and Compounds*, vol. 479, no. 1-2, pp. 290–293, 2009.

[7] B. Li and Y. Wang, "Facile synthesis and enhanced photocatalytic performance of flower-like ZnO hierarchical microstructures," *Journal of Physical Chemistry C*, vol. 114, no. 2, pp. 890–896, 2010.

[8] D. W. Zeng, C. S. Xie, B. L. Zhu et al., "Controlled growth of ZnO nanomaterials via doping Sb," *Journal of Crystal Growth*, vol. 266, no. 4, pp. 511–518, 2004.

[9] X. Jia, H. Fan, M. Afzaal, X. Wu, and P. O'brien, "Solid state synthesis of tin-doped ZnO at room temperature: characterization and its enhanced gas sensing and photocatalytic properties," *Journal of Hazardous Materials*, vol. 193, pp. 194–199, 2011.

[10] E. Pál, V. Hornok, A. Oszkó, and I. Dékány, "Hydrothermal synthesis of prism-like and flower-like ZnO and indium-doped ZnO structures," *Colloids and Surfaces A*, vol. 340, no. 1–3, pp. 1–9, 2009.

[11] B. Wang, M. J. Callahan, C. Xu, L. O. Bouthillette, N. C. Giles, and D. F. Bliss, "Hydrothermal growth and characterization of indium-doped-conducting ZnO crystals," *Journal of Crystal Growth*, vol. 304, no. 1, pp. 73–79, 2007.

[12] C. Jing, Y. Jiang, W. Bai, J. Chu, and A. Liu, "Synthesis of Mn-doped ZnO diluted magnetic semiconductors in the presence of ethyl acetoacetate under solvothermal conditions," *Journal of Magnetism and Magnetic Materials*, vol. 322, no. 16, pp. 2395–2400, 2010.

[13] C. Karunakaran, P. Gomathisankar, and G. Manikandan, "Preparation and characterization of antimicrobial Ce-doped ZnO nanoparticles for photocatalytic detoxification of cyanide," *Materials Chemistry and Physics*, vol. 123, no. 2-3, pp. 585–594, 2010.

[14] Powder Diffract. File, JCPDS Internat. Centre Diffract. Data, PA 19073–3273, U.S.A., 2001.

[15] M. Dondi, F. Matteucci, and G. Cruciani, "Zirconium titanate ceramic pigments: crystal structure, optical spectroscopy and technological properties," *Journal of Solid State Chemistry*, vol. 179, no. 1, pp. 233–246, 2006.

[16] O. Lupan, L. Chow, L. K. Ono et al., "Synthesis and characterization of ag- or sb-doped zno nanorods by a facile hydrothermal route," *Journal of Physical Chemistry C*, vol. 114, no. 29, pp. 12401–12408, 2010.

[17] Y. Yang, J. Qi, Q. Liao, Y. Zhang, L. Tang, and Z. Qin, "Synthesis and characterization of Sb-doped ZnO nanobelts with single-side zigzag boundaries," *Journal of Physical Chemistry C*, vol. 112, no. 46, pp. 17916–17919, 2008.

[18] P. Li, S. Wang, J. Li, and Y. Wei, "Structural and optical properties of Co-doped ZnO nanocrystallites prepared by a one-step solution route," *Journal of Luminescence*, vol. 132, no. 1, pp. 220–225, 2012.

[19] R. B. Peterson, C. L. Fields, and B. A. Gregg, "Epitaxial chemical deposition of ZnO nanocolumns from NaOH solutions," *Langmuir*, vol. 20, no. 12, pp. 5114–5118, 2004.

[20] Y. Zeng, T. Zhang, L. Wang, and R. Wang, "Synthesis and ethanol sensing properties of self-assembled monocrystalline ZnO nanorod bundles by poly(ethylene glycol)-assisted hydrothermal process," *Journal of Physical Chemistry C*, vol. 113, no. 9, pp. 3442–3448, 2009.

[21] Z. L. Wang, "Novel zinc oxide nanostructures discovery by electron microscopy," *Journal of Physics*, vol. 26, no. 1, pp. 1–6, 2006.

[22] A. Phuruangrat, T. Thongtem, B. Kuntalue, and S. Thongtem, "Microwave-assisted synthesis and characterization of rose-like and flower-like zinc oxide nanostructures," *Journal of Ovonic Research*, vol. 7, pp. 107–113, 2011.

[23] J.-S. Liu, J.-M. Cao, Z.-Q. Li, G.-B. Ji, and M.-B. Zheng, "A simple microwave-assisted decomposing route for synthesis of ZnO nanorods in the presence of PEG400," *Materials Letters*, vol. 61, no. 22, pp. 4409–4411, 2007.

[24] Y. Lei, G. Zhao, M. Liu, Z. Zhang, X. Tong, and T. Cao, "Fabrication, characterization, and photoelectrocatalytic application of ZnO nanorods grafted on vertically aligned TiO_2 nanotubes," *Journal of Physical Chemistry C*, vol. 113, no. 44, pp. 19067–19076, 2009.

[25] H. Li, D. Wang, H. Fan, T. Jiang, X. Li, and T. Xie, "Synthesis of ordered multivalent Mn-TiO_2 nanospheres with tunable size: a high performance visible-light photocatalyst," *Nano Research*, vol. 4, no. 5, pp. 460–469, 2011.

[26] H. Chang and M.-H. Tsai, "Synthesis and characterization of ZnO nanoparticles having prism shape by a novel gas condensation process," *Reviews on Advanced Materials Science*, vol. 18, no. 8, pp. 734–743, 2008.

[27] J. Zhao, L. Wang, X. Yan et al., "Structure and photocatalytic activity of Ni-doped ZnO nanorods," *Materials Research Bulletin*, vol. 46, no. 8, pp. 1207–1210, 2011.

[28] J. H. Zeng, B. B. Jin, and Y. F. Wang, "Facet enhanced photocatalytic effect with uniform single-crystalline zinc oxide nanodisks," *Chemical Physics Letters*, vol. 472, no. 1–3, pp. 90–95, 2009.

[29] R. Jain and S. Sikarwar, "Photodestruction and COD removal of toxic dye erioglaucine by TiO_2-UV process: influence of operational parameters," *International Journal of Physical Sciences*, vol. 3, no. 12, pp. 299–305, 2008.

[30] J. Chanathaworn, C. Bunyakan, W. Wiyaratn, and J. Chungsiriporn, "Photocatalytic decolorization of basic dye by TiO_2 nanoparticle in photoreactor," *Songklanakarin Journal of Science and Technology*, pp. 203–210, 2012.